J. Plasma Physics (2000), *vol.* 64, *part* 1, *pp.* 41–55. Printed in the United Kingdom
© 2000 Cambridge University Press

The evolution of magnetic flux ropes in sheared plasma flows

J. M. SCHMIDT and P. J. CARGILL

Space and Atmospheric Physics, The Blackett Laboratory, Imperial College, London SW7 2BZ

(Received 17 July 1999 and in revised form 14 November 1999)

Abstract. The evolution of magnetic flux ropes in a sheared plasma flow is investigated. When the magnetic field outside the flux rope lies parallel to the axis of the flux rope, a flux rope of circular cross-section, whose centre is located at the midpoint of the shear layer, has its shape distorted, but remains in the shear layer. Small displacements of the flux-rope centre above or below the midpoint of the shear layer lead to the flux-rope being expelled from the shear layer. This motion arises because small asymmetries in the plasma pressure around the flux-rope boundary leads to a force that forces the flux rope into a region of uniform flow. When the magnetic field outside the flux rope lies in a plane perpendicular to the flux-rope axis, the flux rope and external magnetic field reconnect with each other, leading to the destruction of the flux rope.

1. Introduction

Magnetic flux tubes and flux ropes are a fundamental building block of solar, solar system and astrophysical plasmas (see e.g. Russell et al. 1990). They are defined as structures in which the magnetic field strength is enhanced over that in the surrounding plasma, and with a length much greater than the width. A typical geometry is a long, straight cylinder. A magnetic flux tube is a structure in which the magnetic field lines are approximately straight, while in a flux rope the field lines are twisted, implying that field-aligned currents are present.

Flux tubes and flux ropes are the dominant magnetic structure in the solar convection zone and photosphere; in the latter region they are the main source of the large-scale solar magnetic field (see e.g. Solanki 1993). The solar corona is comprised of loop structures, which are widely believed to be mini-atmospheres confined in a localized flux rope (see e.g. Kano and Tsuneta 1995). Solar prominences, which are cool structures that survive in the hot corona, are now believed to have magnetic flux ropes as an integral part of their structure (see e.g. Low 1994). The visible prominence occupies only a tiny part of the flux rope, with the rest being barely visible owing to the low plasma density therein. It is widely believed that the flux ropes associated with prominences can be unstable and erupt outward into space (see e.g. Low 1994). Such eruptions (called coronal mass ejections: CMEs) lead to the ejection of $> 10^{12}$ kg of plasma. The magnetic flux ropes associated with CMEs have been detected in the interplanetary medium by spacecraft instruments that can measure their plasma and field properties. In this context, the flux ropes have been termed magnetic clouds and have been observed in space both at the orbit

https://doi.org/10.1017/S0022377800008394 Published online by Cambridge University Press

of the Earth, and at much larger distances and higher latitudes by instruments on the Ulysses spacecraft (see e.g. Burlaga et al. 1988; Gosling et al. 1998).

The equilibrium structure and linear stability of isolated magnetic flux ropes is reasonably well understood at the present time (see papers in Russell et al. 1990). However, despite its obvious importance for many problems in solar and space plasmas, the interaction of flux ropes with complex non-uniform surroundings is only beginning to be explored. For example, the gradual rise of magnetic flux ropes through the solar convection region, and their explosive emergence through the solar photosphere, involves the interaction of a flux rope with a highly stratified medium (see e.g. Chou and Fisher 1989; Shibata et al. 1990). The motion of a flux rope that is being swept into the boundaries between the surface solar granulation involves its interaction with a sheared plasma flow. Similarly, the motion of a CME through the solar wind may involve the interaction of a flux rope with a complex flow pattern (Odstrcil and Pizzo 1999). The focus of this paper is on the latter two scenarios: the behaviour of flux ropes in sheared plasma flows.

While it is tempting to understand the interaction of a flux rope with plasma flows in terms of the theory of a rigid cylinder moving through a fluid, such an approach is misleading. When a rigid body moves through a fluid, the body responds to the relative motion by shedding vortices, leading to a retardation of its motion (a drag force). Obviously the shape and internal properties of such a rigid body are unaltered. However, a flux rope undergoing the same interaction needs to be considered in a different light. A flux rope is a *compressible magnetic structure* whose structure can be influenced by its interaction with a plasma flow. For example, its shape can change, and it can even be destroyed under some conditions.

We began to explore these issues some time ago by studying the interaction of a uniformly accelerated magnetic flux rope with an ambient plasma (Cargill et al. 1995, 1996). It was shown that the flux rope and the plasma interacted with each other, leading to a distortion of the flux rope from its initially circular cross-section. In addition, the flux rope experienced the expected drag force, and, for the first time, drag forces for the MHD regime were determined quantitatively.

This paper addresses a different aspect of the interaction of a flux rope with an ambient plasma, namely its evolution in a sheared plasma flow. We shall apply the work presented here elsewhere to CMEs in particular, so that the focus is on understanding the physical processes that occur. Section 2 of the paper discusses briefly the model used. Section 3 presents a range of results for flux ropes in sheared flows and Sec. 4 presents the conclusions.

2. Description of model and simulation techniques

To study the evolution of a magnetic flux rope in a sheared plasma flow, we solve the equations of compressible magnetohydrodynamics numerically. In conservative form, these are

$$\frac{\partial \rho}{\partial t} + \boldsymbol{\nabla} \cdot (\rho \mathbf{V}) = 0, \tag{2.1}$$

$$\frac{\partial (\rho \mathbf{V})}{\partial t} + \boldsymbol{\nabla} \cdot \left(\rho \mathbf{V}\mathbf{V} + \mathbf{I} P_T - \frac{\mathbf{B}\mathbf{B}}{4\pi} \right) = 0, \tag{2.2}$$

$$\frac{\partial \mathbf{B}}{\partial t} + \boldsymbol{\nabla} \cdot (\mathbf{V}\mathbf{B} - \mathbf{B}\mathbf{V}) = 0, \tag{2.3}$$

https://doi.org/10.1017/S0022377800008394 Published online by Cambridge University Press

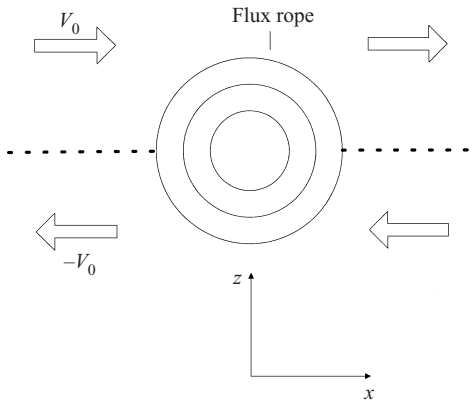


Figure 1. A sketch of the initial conditions used in the simulations. The flux rope is shown by the circular lines, with the plasma flow directed leftward (rightward) below (above) it.

$$\frac{\partial E}{\partial t} + \boldsymbol{\nabla} \cdot \left[(E + P_T)\mathbf{V} - \mathbf{B}\frac{\mathbf{B} \cdot \mathbf{V}}{4\pi} \right] = 0, \tag{2.4}$$

where P_T is the total (thermal and magnetic pressure), defined as

$$P_T = p + \frac{B^2}{8\pi}, \tag{2.5}$$

and E is the total energy,

$$E = \frac{1}{2}\rho V^2 + \frac{p}{\gamma - 1} + \frac{B^2}{8\pi} \tag{2.6}$$

Other symbols have their usual meanings.

The adopted model is quite simple, as shown in Fig. 1. The flux rope is positioned with its axis out of (or into) the plane of the figure (the y direction), with its centre at $x = z = 0$. Outside the flux rope, we examine two possible magnetic field configurations. It is assumed initially that the external magnetic field has only a y component. This is relaxed in Sec. 3.1 to include the case when the external field lies in the (x, z) plane. The plasma pressure and density are uniform inside and outside the flux rope, though they need not be the same in both regions. Details are given in Sec. 3.

The flux rope magnetic field is assumed to take the following form:

$$\mathbf{B} = (0, J_1(r/a), J_0(r/a)), \tag{2.7}$$

which is the familiar Lundquist field in cylindrical polar coordinates (r, θ, y), with the origin at the centre of the flux rope. Here J_0 and J_1 are the zeroth- and first-order Bessel functions and $r^2 = x^2 + z^2$, $\theta = \tan^{-1}(z/x)$. The edge of the flux rope is located at $r = a$, the first zero of $J_0(r/a)$. The pressure inside the flux rope is chosen such that the total (gas plus magnetic) pressure is continuous across its boundaries.

The initial plasma flow is assumed to be only in the x direction at large distances from the flux rope (i.e. from left to right and right to left in Fig. 1), with a reversal in the flow at $z = 0$. The magnitude of the flow is $\pm V_0$, with the flow in the positive x direction when $z > 0$. The plasma flow reverses smoothly across the line $z = 0$, and is assumed to be a hyperbolic tangent:

$$V_x(z) = V_0 \tanh(z/z_c), \tag{2.8}$$

where z_c is a free parameter.

https://doi.org/10.1017/S0022377800008394 Published online by Cambridge University Press

The MHD equations are solved using a 2.5-dimensional flux-corrected transport (FCT) code, based on algorithms discussed in Zalesak (1979) and DeVore (1991). The code uses Cartesian coordinates, and has been discussed by us elsewhere (Cargill et al. 1996, 1997). The numerical simulations are performed in the (x, z) plane. However, magnetic fields and plasma flows are permitted in the y direction. There are 200 cells in the x direction and 100 cells in the z direction, with each grid cell being square. Thus the simulation box extends for twice as far in the x as in the z direction. We found that this was necessary to prevent the left- and right-hand boundaries influencing the results in some of our calculations.

All results are presented in dimensionless units. The origin of the coordinate system is the centre of the simulation box, and so we define the z direction to run from -1 to $+1$ and the x direction to run from -2 to $+2$. Velocities are normalized with respect to the initial (constant) sound speed in the plasma outside the flux rope (defined as C_{s0}), and times to the sound transit time across the flux rope ($2a/C_{s0}$). With this set of units, the plasma beta ($\beta = 8\pi p/B^2$) in the external medium is an important dimensionless parameter.

3. Results

As an example of the type of results that have been obtained, we describe first the case of a flux rope placed in a plasma with a weak y magnetic field. There is no external magnetic field in the (x, z) plane. The centre of the flux rope (i.e. the location of its maximum magnetic field) is located at $x = z = 0$. In dimensionless units, we set $V_0 = 0.75$, $a = 0.25$ and $z_c = 0.05 = a/5$, and the plasma beta outside the flux rope is taken as 10. The plasma pressure inside the flux rope is taken to be 50% of that outside, and the plasma density inside and outside are assumed to be the same. When combined with the need for total pressure balance across the boundary of the flux rope, these parameters lead to quite small values of the plasma beta inside the flux rope (the minimum value is 0.26). Thus the system we are simulating is a flux rope with a strong magnetic field embedded in a high-beta plasma. This corresponds to the situation encountered with interplanetary magnetic clouds in the solar wind.

This system was followed for 12 dimensionless time units. Figure 2 shows the flux-rope magnetic field lines projected on the (x, z) plane at four times early in the simulation. For clarity, only the part of the simulation box around the flux rope is shown (60 cells in each direction). At the start of the simulation, the initial flow evolves into one that 'separates' at the top and bottom of the flux rope: this is the well-known hydrodynamic phenomenon where a high-Reynolds-number flow cannot flow laminarly around a cylindrical or spherical boundary. Such a flow pattern leads to a force on the upper and lower parts of the flux rope that tries to pull them in opposite directions (second panel in Fig. 2). These forces can be parametrized in terms of an aerodynamic drag force, $F_D \propto C_D \rho_e V^2 A$ where ρ_e is the density of the plasma outside the flux rope, V the relative flow speed, A the cross-sectional area of the flux rope exposed to the flow and C_D a dimensionless drag coefficient, typically of order unity for MHD flows (Cargill et al. 1995, 1996).

In the absence of flux-rope magnetic field components in the (x, z) plane (i.e. a flux tube), the drag forces tear the flux rope into two parts. There is no force associated with the flux-rope magnetic field that can counteract the drag forces. However, the evolution differs significantly when there is a flux-rope magnetic field

https://doi.org/10.1017/S0022377800008394 Published online by Cambridge University Press

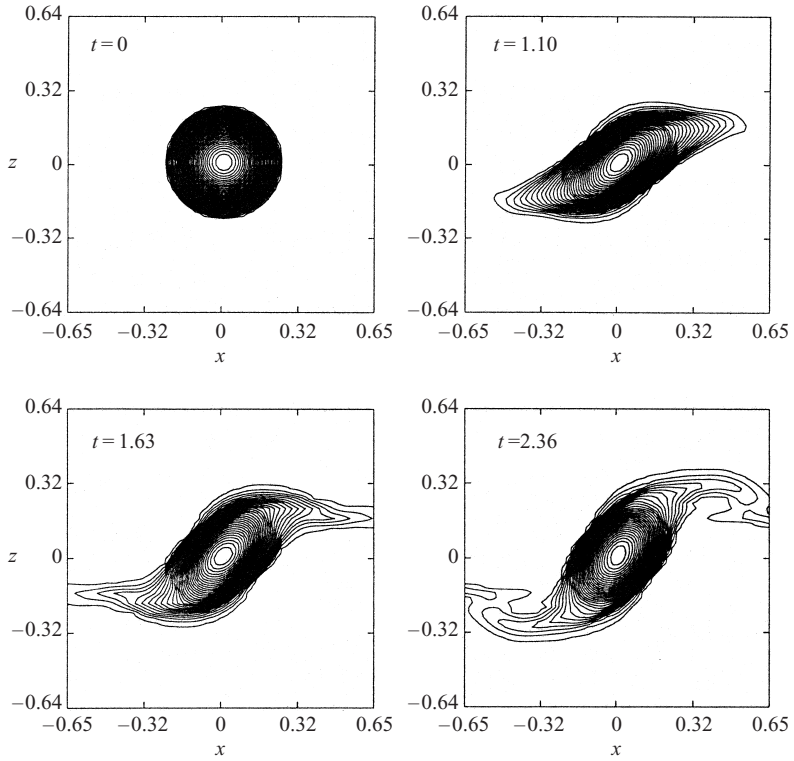


Figure 2. Flux-rope magnetic field lines projected in the (x, z) plane at four times early in a simulation where the maximum flux-rope field is located at $x = z = 0$. Other parameters are $V_0 = 0.75$ and $z_c = 0.05$. Time is measured in units of the sound travel time across the flux rope.

in the (x, z) plane, as is the case here. As the flux rope is stretched out, magnetic tension forces associated with its magnetic field resist the stretching, and attempt to restore its circular shape. Figure 2 shows that they are partially successful in this. The flux rope is not torn apart, and a quasi-equilibrium between tension and drag forces has been established.

Figure 3 shows the flow pattern around the flux rope at the same time as the final panel of Fig. 2. The magnetic field lines are shown as solid lines and the flow is represented by the arrows, whose lengths are proportional to the flow magnitude. Clearly the flux rope acts as an obstacle to the flow, with a magnetic rigidity associated with the tension forces. On the trailing edges above and below the flux rope (upper right and lower left in Fig. 3), vortices have formed, each having a clockwise sense of rotation. (Note that for a flux rope placed in a unidirectional flow, a pair of vortices will eventually form behind the flux rope (Cargill et al. 1995, 1996).) To understand the vortex formation process, consider the vortex to the right of the flux rope. This vortex is due to plasma from the left being displaced upward and over the flux rope, and plasma from the right moving upward to fill the cavity in the wake of the flux rope. This is the expected response of an obstacle being placed in such a flow, except that in this instance the obstacle becomes distorted by the interaction.

Figure 4 shows contour plots of the quantity $p(x, z, t)/p_0 - 1$, where p_0 is the initial plasma pressure *outside* the flux rope. The times of each panel are the same

https://doi.org/10.1017/S0022377800008394 Published online by Cambridge University Press

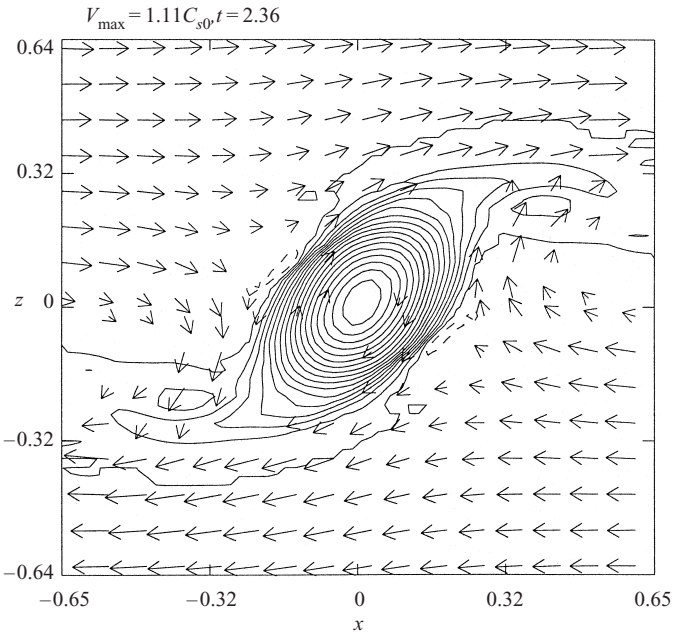


Figure 3. Flux-rope magnetic field lines projected in the (x, z) plane at the same time as the last panel in Fig. 2. Superposed on the field lines are arrows representing the plasma flow. The direction in which the arrows point corresponds to the direction of the flow, and the length of the arrows is proportional to the flow magnitude. All parameters are the same as in Fig. 2.

as in Fig. 2. Solid (dotted) lines correspond to pressures larger (smaller) than p_0. At the start of the interaction, a pair of shocks propagate to top left and bottom right. They leave the system and play no further role in the evolution of the flux rope. As the plasma from the left interacts with the upper half of the flux rope, a compression forms upstream of the leading edge, and a rarefaction downstream of the trailing edge (see third and fourth panels). The same happens on the lower side. As we shall show, the pressure distribution around the boundary of the flux rope plays a critical role in its stability. In the present case, the pressure distribution around the boundary is such as to maintain the flux rope at its original location. It remained there for the duration of this simulation.

To test the stability of a flux rope in sheared flow, the centre was displaced by one grid point in the negative z direction so that it was at $(x, z) = (0, -0.02)$. The evolution was then followed for the same time as before. Figure 5 shows the flux-rope magnetic field lines in the (x, z) plane at four different times, where 100 cells in both the x and z directions are shown. The flux rope is expelled from its initial position downward into the region of leftward-flowing plasma. The characteristic timescales for this expulsion is a few dimensionless time units. The solid lines in Figure 6 shows the x (left) and z (right) positions of the centre of the flux rope as a function of time for $z_c = 0.05$. The centre is defined as being the location of maximum y vector potential. The flux rope initially remains in the shear flow, undergoing some small displacements, but after about 2–3 dimensionless time units, it rapidly moves downward. The motion after leaving the sheared flow is at roughly constant velocity.

https://doi.org/10.1017/S0022377800008394 Published online by Cambridge University Press

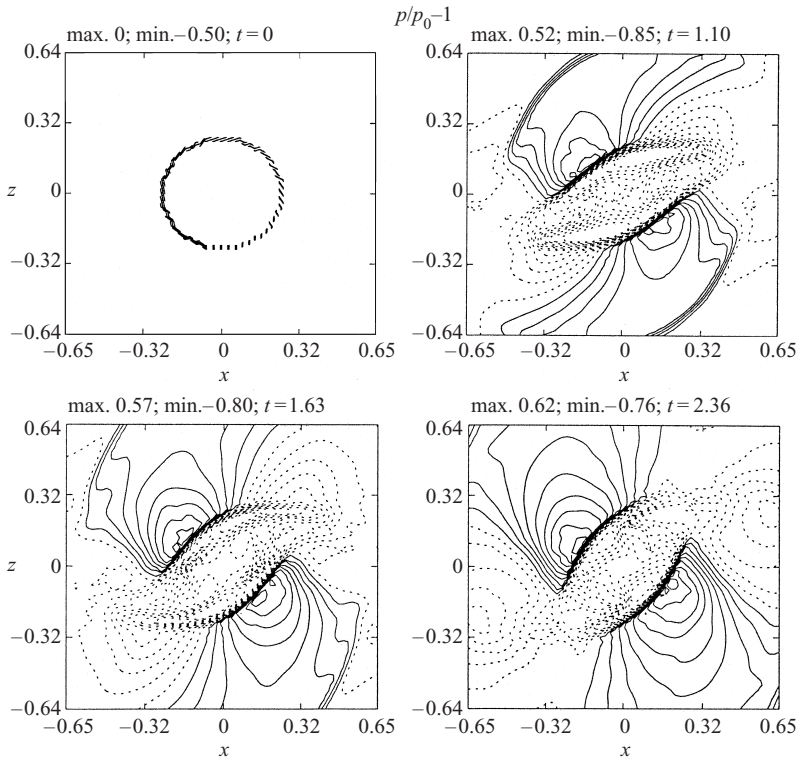


Figure 4. Contours of the quantity $p(x, z, t)/p_0 - 1$ at the same times as shown in Fig. 2.

To examine this expulsion further, we performed a second simulation in which the centre of the flux tube was initially located one cell *above* the centre of the shear layer. In this case, the flux rope moved toward the upper right-hand corner of the simulation box. The conclusion is that a flux rope placed in a sheared flow is unstable to small (but not infinitesimal) perturbations. (Note that we use the word 'instability' here to describe the fact that a large-scale structure will move from an equilibrium position if it is perturbed. This should be contrasted with the use of the word 'instability' in many areas of plasma physics, where a fragmentation or destruction of an equilibrium is implied.)

We investigated the effect of varying the width of the shear layer by changing the parameter z_c. The dashed and dash-dotted lines in Fig. 6 show $z_c = 0.125$ and 0.25 respectively. Clearly the broader the layer, the longer it takes for the flux rope to be expelled. However, in each case, the flux rope is unstable.

The mechanism for instability has been identified as follows. If the flux rope initially has its centre slightly below the centre of the shear layer, the drag force on the lower part exceeds that on the upper part, since the drag force is proportional to the cross-sectional area exposed to the flow. This force imbalance moves the flux rope to the left initially (see Fig. 6a), but does not lead to immediate motion in the negative z direction. As a consequence of this motion in the x direction, the flow relative to the upper half increases, and that with respect to the lower half decreases. This motion results in a pressure distribution around the boundary that

https://doi.org/10.1017/S0022377800008394 Published online by Cambridge University Press

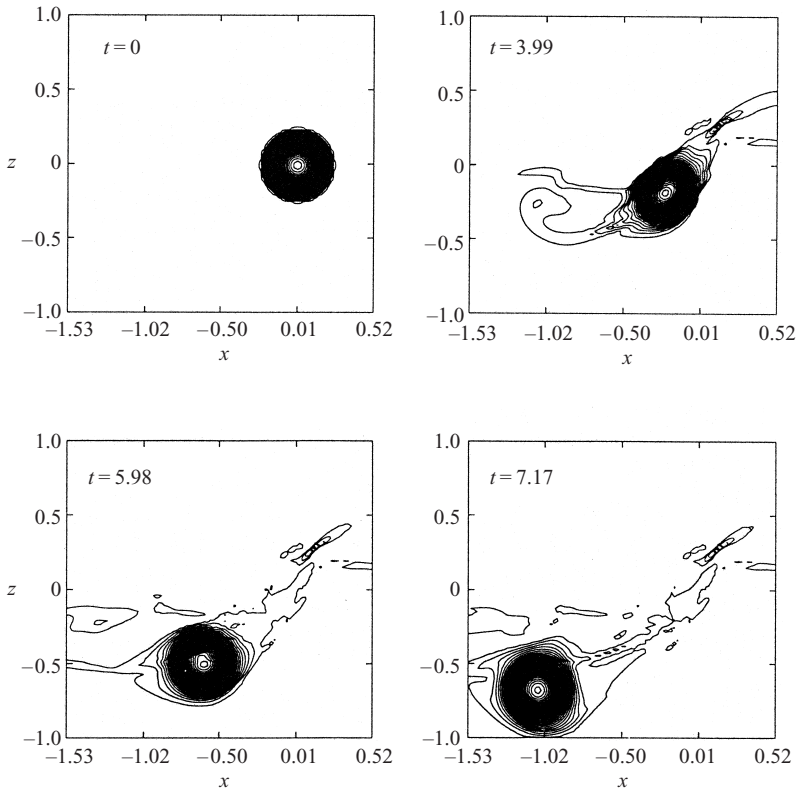


Figure 5. Flux-rope magnetic field lines projected on the (x, z) plane at four times, showing the instability of the flux rope when it is displaced a small distance from the shear layer. The initial parameters are the same as those in Fig. 2.

loses the symmetry needed to maintain the flux rope in its initial position. Figure 7 shows $p(x, z, t)/p_0 - 1$ at similar times to Fig. 4. The lower right panel shows a reduction in the pressure enhancement at the lower left end of the flux rope. When the total force due to the pressure fluctuations is summed around the boundary, there is then a net force that pushes the flux rope towards the bottom left of the simulation box.

In addition to z_c, the two most important parameters governing the behaviour of the flux rope are V_0 and the ratio of densities inside (ρ_i) and outside (ρ_e) the flux rope. Figure 8 summarizes the results for both these parameters. Figure 8(a,b) show the position of the centre of the flux rope for three different values of ρ_i/ρ_e. The solid, dashed and dash-dotted lines have ρ_i/ρ_e = 1, 5 and 0.2 respectively. Decreasing (increasing) the flux-rope density leads to it being expelled more (less) rapidly. This can be readily understood by noting that the smaller the inertia of the flux rope, the more easily can it respond to pressure forces acting on it.

Figure 8(c,d) show the effect of varying V_0. The solid, dashed and dash-dotted curves show V_0/C_{s0} = 0.75, 0.375 and 1.5 respectively. As would be expected, larger flow speeds lead to faster expulsion, since the pressure forces around the flux rope should scale as V_0^2.

https://doi.org/10.1017/S0022377800008394 Published online by Cambridge University Press

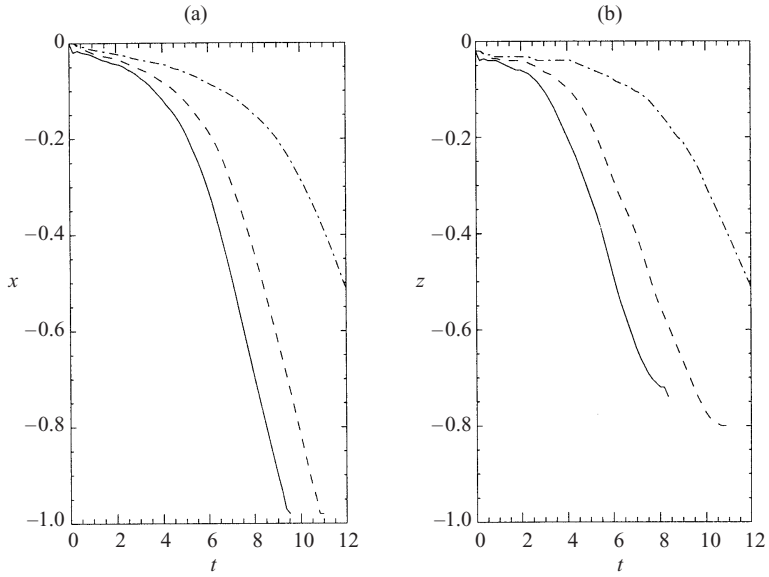


Figure 6. The x (a) and z (b) positions of the flux rope as it moves away from the shear later as a function of time. The solid, dashed and dash-dotted lines show $z_c = 0.05$, 0.125 and 0.25 respectively.

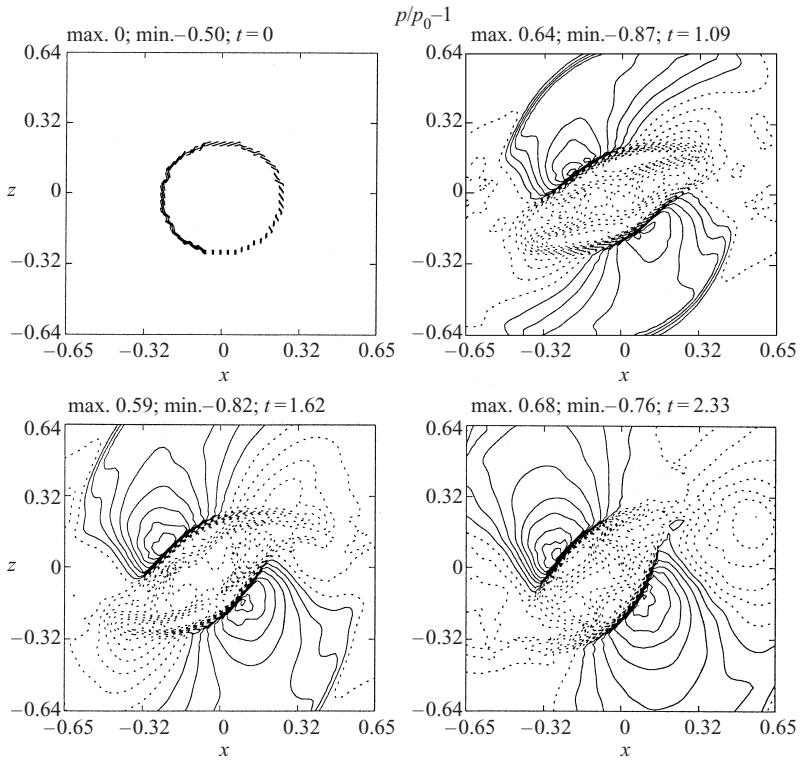


Figure 7. Contours of the quantity $p(x, z, t)/p_0 - 1$ for the early part of the simulation shown in Fig. 5.

https://doi.org/10.1017/S0022377800008394 Published online by Cambridge University Press

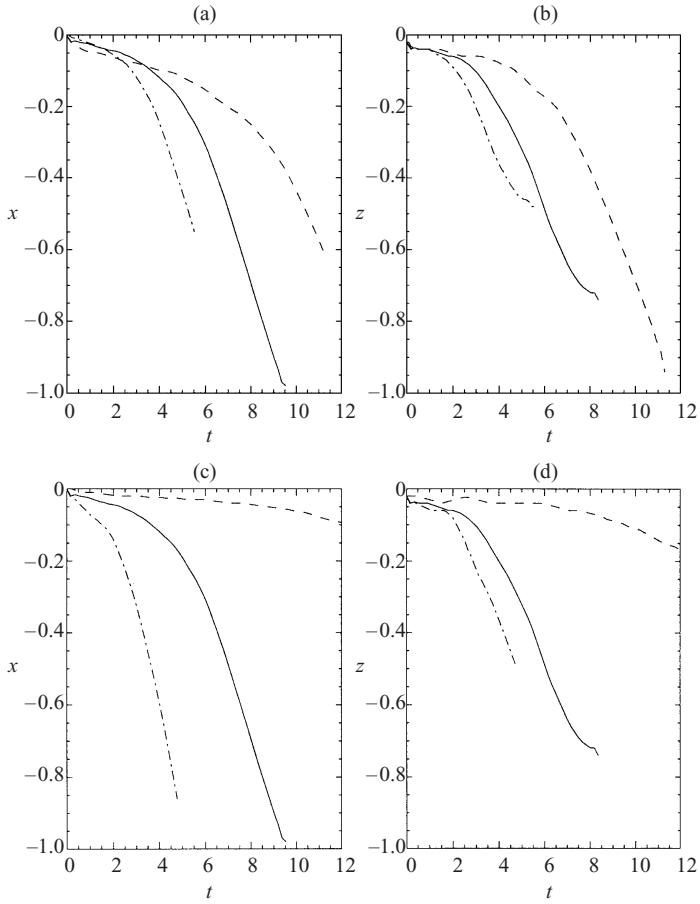


Figure 8. (a) and (b) show the x (a) and z (b) position of the flux rope as it moves away from the shear layer as a function of time for ρ_i/ρ_e = 1, 5 and 0.2 for solid, dashed and dash-dotted lines respectively. (c) and (d) show the positions for V_0 = 0.75, 0.375 and 1.5 denoted by solid, dashed and dash-dotted lines respectively.

3.1. External magnetic field in the (x, z) *plane*

We examined the case when there was a unidirectional magnetic field lying in the (x, z) plane. This introduces two new (and competing) effects. The first is that the tension force associated with the external magnetic field would be expected to resist any motion of the flux rope away from its initial position, confining it to the shear layer, and so suppressing the instability discussed above. However, the second effect is that for an asymptotically unidirectional external field, there will always be a location where the flux rope and external field lines are oppositely directed. Magnetic reconnection can then occur, and potentially lead to the destruction of the flux rope. (In fact, our earlier work (Cargill et al. 1996) that looked at the motion of a flux rope in a magnetized plasma suggested that magnetic reconnection between the flux rope and the external field could take place, albeit rather slowly, so that the topological integrity of the flux rope survived over many sound transit times.)

To assess these competing effects, we have carried out simulations of the evolution of a magnetic flux rope in a sheared plasma flow in the presence of a magnetic field

https://doi.org/10.1017/S0022377800008394 Published online by Cambridge University Press

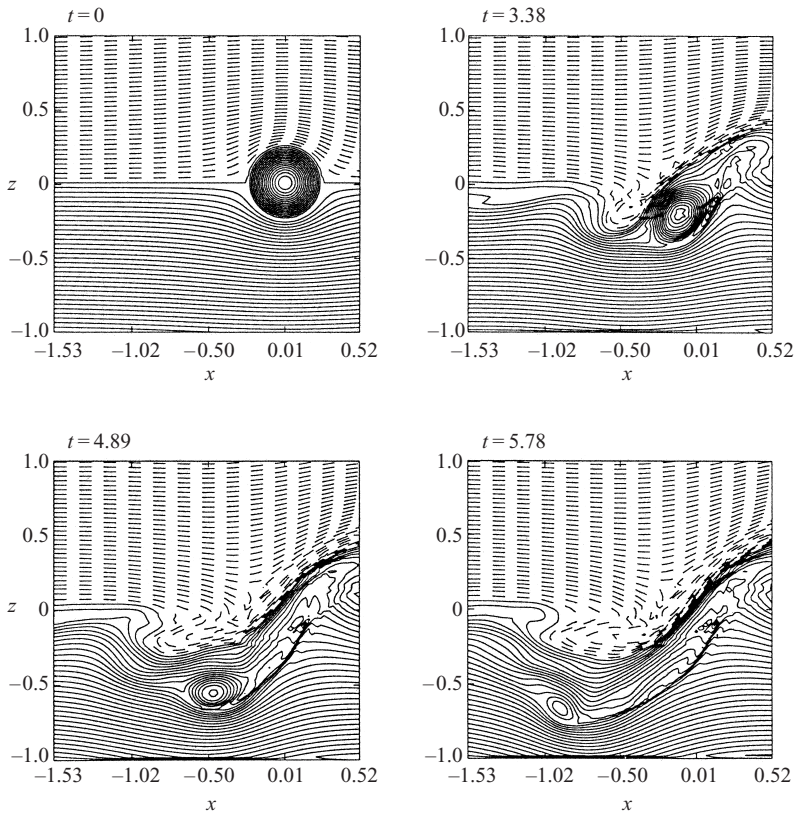


Figure 9. Magnetic field lines projected on the (x, z) plane at four times for a case when the magnetic field outside the flux rope lies in the (x, z) plane. Solid (dashed) field lines have positive (negative) values of A_y. The magnetic field inside the flux rope has a counterclockwise sense of rotation. At large values of $|x|$ and $|z|$, the field points in the negative x direction.

in the (x, z) plane. The external magnetic field is assumed to be deformed by the presence of the flux rope, and can be described in terms of a vector potential

$$A_y = B_0 a\left(\frac{r}{a}\right)\left(\frac{a^2}{r^2} - 1\right) \sin\theta, \tag{3.1}$$

where the cylindrical coordinate system was defined in Sec. 2. The upper left panel of Fig. 9 shows the initial topology of the magnetic field lines in the (x, z) plane. At large values of $|x|$ and $|z|$, the field points in the negative x direction. Solid (dashed) lines correspond to positive (negative) values of the vector potential. We use this notation to emphasize the magnetic reconnection phenomenon and the original position of the field lines (see also Cargill et al. 1996). Total pressure balance is enforced across the flux-rope boundary at $\theta = \pi/2, 3\pi/2$. It is impossible to have total pressure balance across the boundary of a flux rope for all values of θ for such an external field (Pneuman 1983; Cargill et al. 1996). We now set $\beta = 1$ at large distances from the flux rope. Inside the flux rope, the minimum value of β is 0.18. β is chosen to be smaller than in the previous examples in order to assess the role that magnetic tension forces play in confining the flux rope. Finally, the next pair

https://doi.org/10.1017/S0022377800008394 Published online by Cambridge University Press

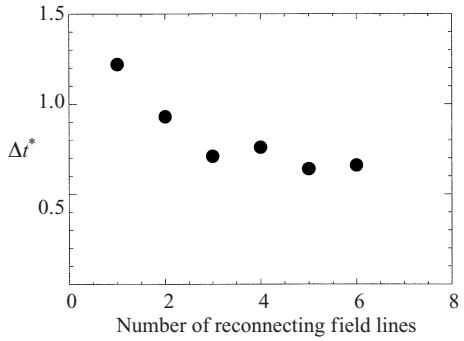


Figure 10. The elapsed time between equally spaced field lines in the flux rope reconnecting with the external magnetic field. Time is measured in units of $2a/C_{s0}$.

of simulations have the flux rope located at the centre of the shear layer. In Sec. 3, we showed that this was a stable initial condition with no external (x, z) field.

The results depend on the sense of rotation of the magnetic field in the flux rope. Figure 9 shows a case with a counterclockwise rotation of the flux-rope field, so that antiparallel fields occur along the lower boundary of the flux rope. The evolution (and ultimate destruction) of such a flux rope is shown in the four panels of Fig. 9. Initially, the flow is displaced around the flux rope as before, but now there is a small amount of magnetic reconnection on the lower side. This leads to a net magnetic pressure force that pushes the flux rope downward (Cargill et al. 1996, p. 4865), driving the antiparallel field lines together. The centre of the flux rope is no longer at the centre of the shear layer, so that the hydrodynamic effects discussed in the previous section now become important, pushing the flux rope downward, and driving together regions of oppositely directed magnetic field. The remaining panels of Fig. 9 show that this forcing leads to the rapid destruction of the flux rope: in the last panel, the flux rope is barely visible.

To see how the reconnection rate changes throughout the simulation, we followed the behaviour of 10 field lines inside the flux rope, and noted when they reconnected with the external field. The field lines corresponded to equally spaced values of the vector potential. Figure 10 shows the time that elapses between the reconnection of each succesive field line, where the time is measured in units of $2a/C_{s0}$. The results were obtained by generating a large number of plots, with a possible error in Δt^* of ± 0.16. The results give credence to the view that the initial reconnection takes place slowly, with the reconnection then speeding up as the hydrodynamic effects drive the flux rope into the external field. We estimate that the reconnection rate in the latter part of the simulation is approximately $0.05V_{ae}$, where V_{Ae} is the Alfvén speed in the external medium.

It is worth stressing that this result is another example of the role that imposed boundary conditions play in driving magnetic reconnection, with the behaviour at the actual reconnection site adjusting to dissipate the field as it is forced in. In these simulations, the only resistivity is numerical (i.e. due to truncation errors arising from the finite-differencing of the MHD equations), so the results do not require any assumption about the form of the resistivity. The tension force that could potentially have resisted the motion of the flux rope away from its initial position can never play a role, because the field lines with which it would have been associated break during the reconnection.

https://doi.org/10.1017/S0022377800008394 Published online by Cambridge University Press

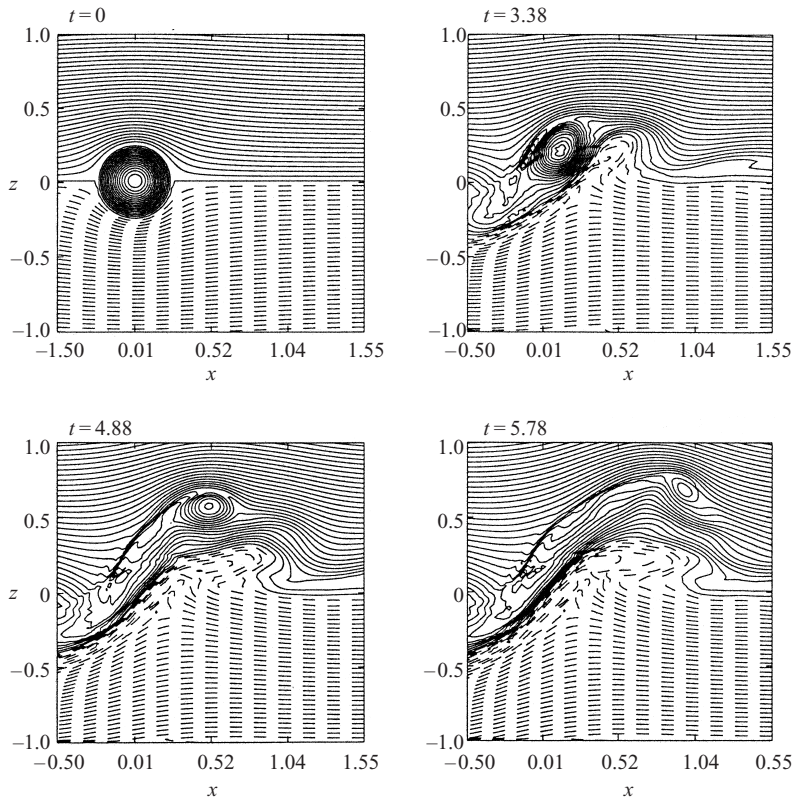


Figure 11. As Fig. 9, except that the flux-rope field lines now have a clockwise sense of rotation. For clarity, solid (dashed) field lines now have negative (positive) values of A_y.

Further understanding of this process can be gained by changing the sense of rotation of the flux rope field to be clockwise while maintaining exactly the same initial location. The results are shown in Fig. 11. The flux rope is now expelled upwards from the shear layer, and is destroyed there. Indeed, the result is almost a mirror image of Fig. 9. Reconnection now begins on the upper side, where the flux rope and external fields are antiparallel, resulting in an initial upward displacement of the flux rope. The hydrodynamic forces then drive further upward motion.

Finally, it is interesting to speculate on what will happen when a flux rope is injected into a current sheet, as is potentially the case in the solar wind (Crooker et al. 1998). One then has antiparallel magnetic fields on both sides for one sense of field rotation, or on neither side for the other. We anticipate that in the former case, destruction of the flux rope will be very rapid. In the latter case, the flux rope can survive for long times.

4. Summary

This paper has examined the magnetohydrodynamic evolution of magnetic flux ropes that are located in a sheared plasma flow. For the case when the magnetic field outside the flux rope is weak, the flux rope position is unstable, and it is expelled from the centre of the shear layer on a timescale of a few sound transit

https://doi.org/10.1017/S0022377800008394 Published online by Cambridge University Press

times. When the magnetic field outside the flux rope is relatively strong, and has a component perpendicular to the flux rope axis, the flux rope is destroyed as its field undergoes magnetic reconnection with the external field.

These results suggest that some rethinking is needed about how magnetic flux ropes behave in variable plasma flows. While our results have been presented for the case of a symmetric sheared flow for computational convenience, the generalization to different relative shears involves a simple change of reference frame.

Thus our conclusion is that magnetic flux ropes in space plasmas will tend not to be found in regions of sheared flow, and further, when a flux rope tries to move into a sheared flow, it will be unable to do so. Depending on the magnetic field orientation and strength, it will either be reflected or destroyed. An important implication of this work is for studies of CMEs in the solar wind – in particular, the question arises whether CMEs that originate at the equatorial streamer belt can penetrate into the high-speed solar wind that exists at higher latitudes. CMEs are seen frequently in the high-speed wind, and some have argued that these originate in the low-speed wind. Spherical geometry is then likely to be an important consideration.

Acknowledgements

The authors thank the UK Particle Physics and Astronomy Council for supporting this work at Imperial College. We also thank Dan Spicer and Steve Zalesak for their work on, and advice about, the simulation codes used in this paper.

References

Burlaga, L. F. 1988 Magnetic clouds and force-free fields with constant alpha. *J. Geophys. Res.* **93,** 7217.

Cargill, P. J., Chen, J., Spicer, D. S. and Zalesak, S. T. 1995 Geometry of interplanetary magnetic clouds. *Geophys. Res. Lett.* **22**, 647–650.

Cargill, P. J., Chen, J., Spicer, D. S. and Zalesak, S. T. 1996 MHD simulations of the motion of magnetic flux tubes through a magnetised plasma *J. Geophys. Res.* **101**, 4855–4870.

Cargill, P. J., Spicer, D. S. and Zalesak, S. T. 1997 MHD simulations of Alfvénic pulse propagation in solar magnetic flux tubes: two dimensional slab geometry. *Astrophys. J.* **488**, 854–866.

Chou, D.-Y. and Fisher, G. H. 1989 Dynamics of anchored flux tubes in the convection zone. 1. Details of the model. *Astrophys. J.* **341**, 533–544.

Crooker, N. U., Gosling, J. T. and Kahler, S. W. 1998 Magnetic clouds at sector boundaries. *J. Geophys. Res.* **103**, 301.

DeVore, R. C. 1991 Flux-corrected transport techniques for multidimensional compressible magnetohydrodynamics. *J. Comput. Phys.* **92**, 142–160.

Gosling, J. T., Riley, P., McComas, D. J. and Pizzo, V. J. 1998 Overexpanding coronal mass ejections at high heliographic latitudes: observations and simulations. *J. Geophys. Res.* **103**, 1941.

Kano, R. and Tsuneta, S. 1995 Scaling law of solar coronal loops obtained with Yohkoh. *Astrophys. J.* **454**, 934–942.

Low, B. C. 1994 Magnetohydrodynamic processes in the solar corona. *Phys. Plasmas* **1**, 1684.

Odstrcil, D. and Pizzo, V. J. 1999 Three dimensional propagation of coronal mass ejections (CMEs) in a structured solar wind flow: 2. CME launched adjacent to the streamer belt. *J. Geophys. Res.* **104**, 493.

Pneuman, G. W. 1983 Ejection of magnetic fields from the Sun: acceleration of a solar wind containing diamagnetic plasmoids. *Astrophys. J.* **265**, 468–482.

Russell, C. T., Priest, E. R. and Lee, L. C. 1990 *Physics of magnetic flux ropes*. AGU Monograph 58.

https://doi.org/10.1017/S0022377800008394 Published online by Cambridge University Press

Shibata, K., Nozawa, S., Matsumoto, R., Sterling, A. C. and Tajima, T. 1990 Emergence of solar magnetic flux from the convection zone into the photosphere and chromosphere. *Astrophys. J. Lett.* **351**, L25–L28.

Solanki, S. K. 1993 Small scale solar magnetic fields: an overview *Space Sci. Rev.* **63**, 1.

Zalesak, S. T. 1979 Fully multidimensional flux-corrected transport algorithms for fluids. *J. Comput. Phys.* **31**, 335–359.

https://doi.org/10.1017/S0022377800008394 Published online by Cambridge University Press